Steady-state sustainment of divertor detachment with multi-species impurity seeding in LHD

Kiyofumi Mukai[1, 2], Suguru Masuzaki[1, 2], Yuki Hayashi[1], Tetsutaro Oishi[1, 2], Chihiro Suzuki[1, 2], Masahiro Kobayashi[1, 2], Tokihiko Tokuzawa[1, 2], Hirohiko Tanaka[3], Kenji Tanaka[1, 4], Toshiki Kinoshita[4], Hikona Sakai[4], Byron Jay Peterson[1, 2]

[1] National Institute for Fusion Science, National Institutes of Natural Sciences, Toki, Japan
[2] The Graduate University for Advanced Studies, SOKENDAI, Toki, Japan
[3] Graduate School of Engineering, Nagoya University, Nagoya, Japan
[4] Interdisciplinary Graduate School of Engineering Sciences, Kyushu University, Kasuga, Japan

E-mail: mukai.kiyofumi@nifs.ac.jp

Abstract

Multi-species impurity seeding is an advanced operation scenario to mitigate the divertor heat load for the realization of future fusion reactors. In the Large Helical Device (LHD), divertor detachment is successfully sustained using higher-Z (krypton, Kr) and lower-Z (neon, Ne) superimposed seeding. Emission from Kr impurities is drastically enhanced if it is followed by Ne seeding. Plasma radiation can be enhanced even at the upstream region in the edge plasma compared with Ne only seeded plasmas with suppression of impurity accumulation toward the central plasma. The characteristics of divertor heat load reduction and energy confinement are comparable between the Kr+Ne seeding and Ne only seeding under the same radiation fraction. However, while the detachment in Ne only seeding is transient, the detachment in Kr+Ne seeding is stable. It indicates that multi-species impurity seeding can be competitive for steady-state operation although further investigation is desired about the balance between divertor heat load reduction, impurity screening, and confinement degradation. The Kr emission enhancement is strongly affected by electron density and temperature at the last closed flux surface resulting in impurity penetration.

Keywords: detachment, divertor, impurity seeding, LHD

1. Introduction

Divertor detachment is a desirable regime to realize a fusion reactor. Divertor heat load should be mitigated stably. Furthermore, to handle the power exhaust, it is necessary to enhance plasma radiation not only in the divertor region but also in the upstream region with suppression of dilution. Therefore, multi species impurity seeding of higher-Z and lower-Z impurities is proposed in JT-60SA [1]. In ASDEX Upgrade, argon (Ar) and nitrogen (N) seeding was performed to feedback control main chamber radiation by Ar seeding and target heat flux by N seeding [2]. In Wendelstein 7-X, detachment using Ne or N seeding has been investigated [3]. In LHD, we have investigated detachment using Ne, N or Kr seeding individually [4-6]. However, the characteristics of divertor detachment in multi-species impurity seeded plasmas have not been investigated. Thus, in this study, we attempted to superimposed seeding using Kr and Ne in LHD. The cooling rate of Ne has the maximum at the electron temperature, T_e, ~ 30 eV. On the other hand, the rate of Kr takes a local minimum at T_e ~ 30 eV, it is expected that these impurities could enhance plasma radiation complementarily.

The rest of the paper consists as follows. The experimental setup is shown in section 2. In section 3, steady-state sustainment of divertor detachment with Kr+Ne seeding is shown and Kr emission enhancement due to Ne seeding is discussed. The paper is summarized in section 5.

2. Experimental setup on LHD

The experimental setup on LHD is shown in FIG. 1. In this study, the magnetic configuration is set with the major radius of the magnetic axis, R_{ax} = 3.60 m. The direction of the toroidal magnetic field is counterclockwise and its strength B_t = 2.75 T. The natural error field is compensated using a perturbation coil system. Plasmas are generated using electron cyclotron heating (ECH) and are sustained using three tangential neutral beam injections (NBIs). Deuterium gas is puffed from the lower port between the toroidal sections #3 and #4 (3.5-L). Impurity gases (Ne and Kr) are puffed from the 5.5-L port. Total plasma radiation, P_{rad}, and radiation brightness profiles are measured by resistive bolometer arrays [7]. Ne and Kr emission profiles are measured with EUV spectroscopy [8] and SOXMOS [9-11]. Divertor heat load is evaluated by Langmuir probe arrays [6].

3. Divertor detachment with multi-species impurity seeding

3.1 Steady-state sustainment of divertor detachment with Kr+Ne seeding

The waveform in Kr and Ne superimposed seeded plasma is shown in FIG. 2. As shown in FIG. 2 (a), the plasma is generated using ECH and is sustained using NBI. Line-averaged electron density, $n_{e, bar}$, shown in FIG. 2 (b), before impurity seeding is 1×10^{19} m^{-3}. Kr is seeded 0.4 s before Ne seeding for 5 ms with the flow rate of 3.0 Pa·m^3/s with the amount of 0.015 Pa·m^3, as shown in FIG. 2 (c). Since the plasma response to Kr is slow compared with Ne, Ne is

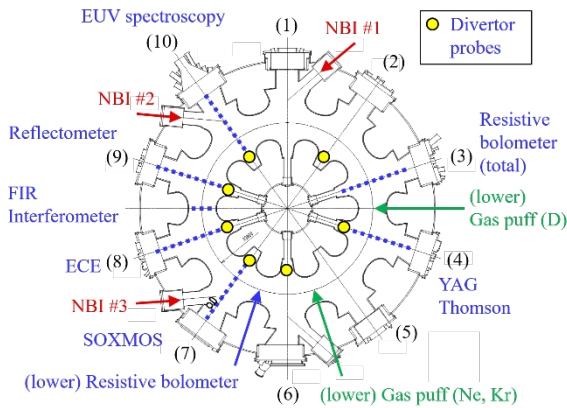seeded 0.4 s after the Kr seeding for 25 ms with the flow rate of 1.8 Pa·m^3/s and with the amount of 0.045 Pa·m^3. After Kr seeding but before Ne seeding, -0.4 s < t - t_{Ne} < 0.0 s, increase of total plasma radiation power, P_{rad}, is insubstantial as shown in FIG. 2 (d). As shown in FIG. 2 (e), Kr emission is slightly enhanced. However, the enhancement of P_{rad} is 0.08 MW and P_{rad} at t - t_{Ne} = 0.0 s is 0.55 MW. $\Sigma I_{sat, all}$ shown in FIG. 2 (f), which is the summation of ion saturation current in all divertor probes, gradually decreased by 10%. $\langle q_{div} \rangle$ shown in FIG. 2 (g), which is the averaged divertor heat flux in all divertor probes, gradually decreases by 20%. $\tau_{E, exp}/\tau_{E, ISS04}$ shown in FIG. 2 (h) gradually decreases and is 0.95 at t - t_{Ne} = 0.0 s. Here, $\tau_{E, exp}$ is experimental energy confinement time calculated by $W_p/(P_{NBI, abs}-dW_p/dt)$ where W_p and $P_{NBI, abs}$ are plasma stored energy and absorbed NBI heating power, respectively. $\tau_{E, ISS04}$ is energy confinement time estimated by ISS04 scaling [12].

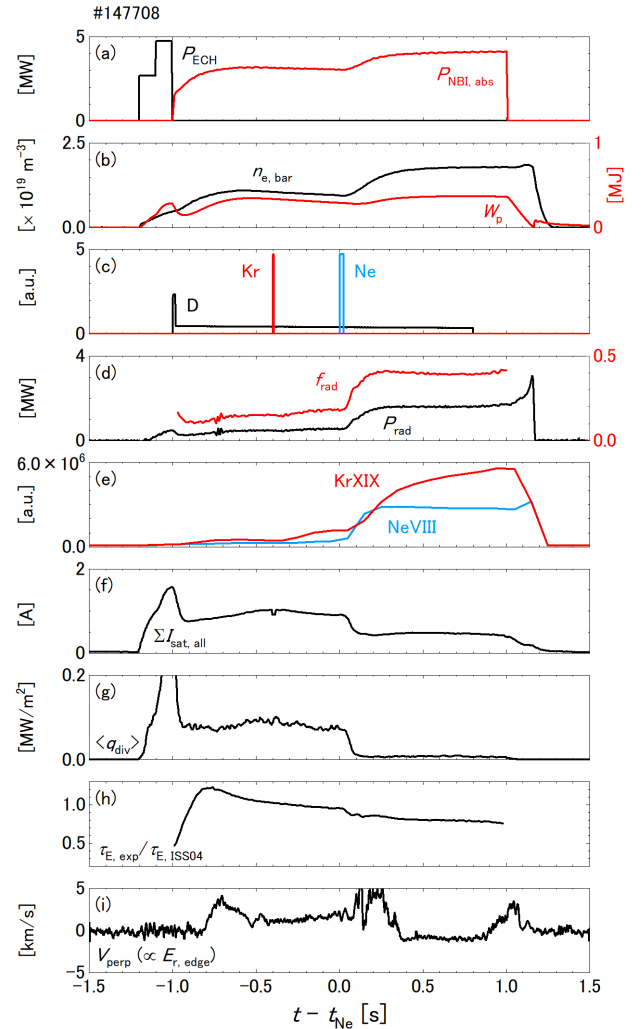The results after the Kr seeding but before Ne seeding

FIG. 2. Steady-state sustainment of divertor detachment for ~ 1 s using Kr+Ne superimposed seeding. Pre-seeded Kr emission is drastically enhanced after Ne seeding.

FIG. 1. Experimental setup on LHD.

indicated that Kr only seeding is not effective for the divertor detachment. However, after the Ne seeding at $t - t_{Ne} = 0.0$ s, ΣI_{sat} and $<q_{div}>$ drastically decreases with the increase of P_{rad}. The detachment is sustained stably until the termination of the NBI heating. The sustainment of the detachment can extend if there is no limitation on the pulse length of the NBI heating. Here, as shown in FIG. 2 (b), $n_{e, bar}$ increases from 0.96×10^{19} m^{-3} (averaged -0.1 s $\leq t - t_{Ne} \leq 0.0$ s) to 1.76×10^{19} m^{-3} (averaged from 0.4 s $\leq t - t_{Ne} \leq 1.0$ s) after the Ne seeding. When the seeded Ne are fully ionized, $n_{e, bar}$ can increase to 0.36×10^{19} m^{-3}. The T_e at the magnetic axis is lower than the ionization energy of KrXXVII, 2.9 keV. Therefore, when each seeded Kr generates 25 electrons, $n_{e, bar}$ can increase to 0.30×10^{19} m^{-3}. Since the total $n_{e, bar}$ increase of 0.80×10^{19} m^{-3} is larger than the increase 0.66×10^{19} m^{-3} due to the impurity seeding, wall recycling should be changed. NBI port-through power is constant, however, the heating efficiency improved by the $n_{e, bar}$ increase. Therefore, $P_{NBI, abs}$ shown in FIG. 2 (a) increases after the Ne seeding. At 0.4 s $\leq t - t_{Ne} \leq 1.0$ s, P_{rad} increases to 1.61 MW and radiation fraction, $f_{rad} = P_{rad}/P_{NBI, abs}$, was 0.40. $<q_{div}>$ averaged 0.4 s $\leq t - t_{Ne} \leq 1.0$ s decreases by 0.92 compared with $<q_{div}>$ averaged -0.5 s $\leq t - t_{Ne} \leq -0.4$ s before the Kr seeding. $\tau_{E, exp}/\tau_{E, ISS04}$ averaged 0.4 s $\leq t - t_{Ne} \leq 1.0$ s was 0.80. Time evolutions of KrXIX and NeVIII emissions shown in FIG. 2 (e) had quite interesting behaviors. After the Ne seeding, not only NeVIII emission but also KrXIX emission is drastically enhanced after $t - t_{Ne} = 0.15$ s. The behavior of the impurities is discussed in the next section.

The waveform of Ne only seeded plasma is shown in FIG. 3. $P_{NBI, abs}$ and $n_{e, bar}$ before the Ne seeding shown in FIG. 3 (a) and (b) were comparable with the Kr+Ne superimposed seeded plasma shown in FIG. 2. Ne is seeded from $t - t_{Ne} = 0.0$ s for 40 ms as shown in FIG. 3 (c) with the flow rate of 1.8 Pa·m^3/s and the amount of 0.072 Pa·m^3. The maximum f_{rad} shown in FIG. 3 (d) is also comparable with those of FIG. 2. In the Ne only seeded plasma, after the Ne seeding $\Sigma I_{sat, all}$ and $<q_{div}>$ reduction with P_{rad} and NeVIII enhancement is observed as shown in FIG. 3 (d) - (g). The most important difference between Kr+Ne and Ne only seeded plasma is that the detachment in Kr+Ne seeded plasma is sustained stably while the detachment in Ne only seeded plasma is transient and is reattached in 0.2 s. In the Ne only seeded plasma, at $t - t_{Ne} = 0.17$ s, f_{rad} had the maximum value of 0.40 which is 10% higher than that in Ne only seeding with multi-pulses [5]. $<q_{div}>$ averaged 0.1 s $\leq t - t_{Ne} \leq 0.25$ s is 0.77 lower compared with that averaged from 0.0 s $\leq t - t_{Ne} \leq 0.1$ s before the Ne seeding as shown in FIG. 3. (g). $\tau_{E, exp}/\tau_{E, ISS04}$ averaged 0.10 s $\leq t - t_{Ne} \leq 0.25$ s shown in FIG. 3 (h) is 0.90.

Magnetic field connection length, L_c, and typical I_{sat} profiles on a divertor plate in Kr+Ne and Ne only plasmas are shown in FIG. 4. The private-side peak of the I_{sat} profile
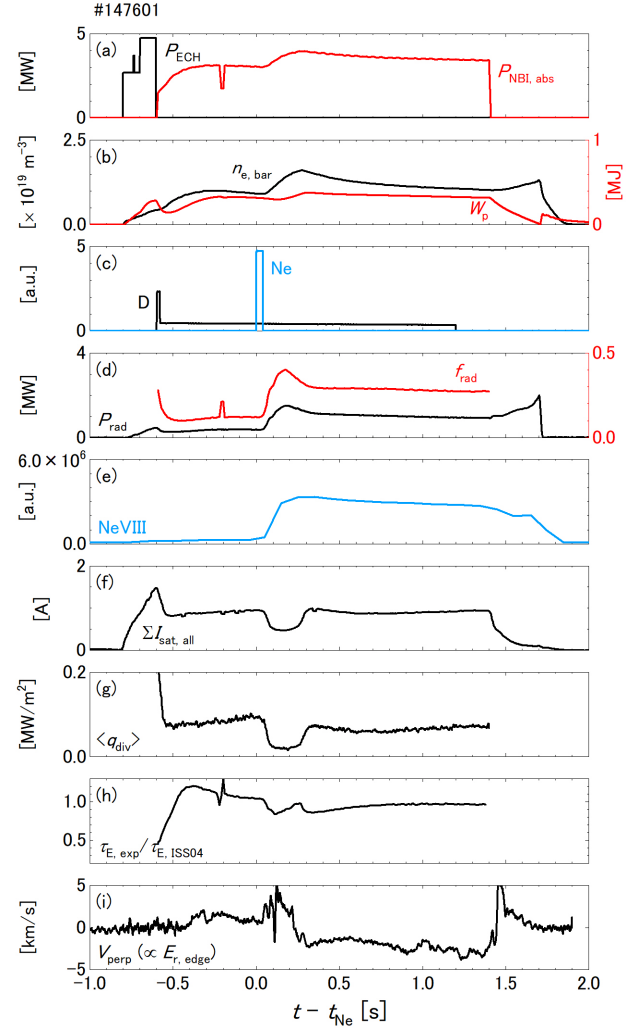

FIG. 3. Divertor detachment using Ne seeding with the maximum $f_{rad} \sim 0.4$ which is comparable with FIG. 2. The detachment disappears 0.2 s after the Ne seeding.

would be attributed to the magnetic field change due to the edge pressure gradient inside the core region [13]. FIG. 5 shows the toroidal profile of the ΣI_{sat} ratio before impurity seeding and after impurity seeding. Here, ΣI_{sat} is the summation of ion saturation current in 40 divertor probes in a toroidal section. In the Kr+Ne plasma, the peak value of ΣI_{sat} slightly decreases. However, the reduction was not significant and I_{sat} increases at some positions on the divertor plate. At this time, the ΣI_{sat} ratio had toroidal asymmetry as shown in FIG. 5. It implies that Kr ions are localized along magnetic field lines connected to the position of impurity seeding and are not expanded to all toroidal sections. The ΣI_{sat} ratio decreases in toroidal sections #2, 7, 8, 9, and 10 while it does not decrease in toroidal sections #4 and 6. Kr and Ne seeding are applied from toroidal section #5.5 as mentioned in section 2. After the Ne seeding, I_{sat} on the divertor plate decreases in both Kr+Ne and Ne only seeded
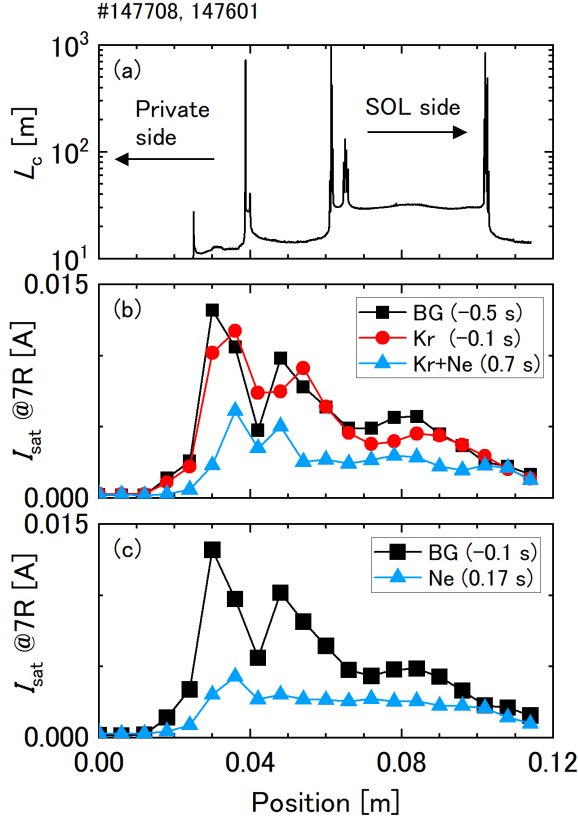
#147708, 147601

FIG. 4. (a) L_c profile on a divertor plate located on the right-side in the toroidal section #7 and typical I_{sat} profiles in the (b) Kr+Ne seeded plasma and (c) Ne only seeded plasma. After the Ne seeding, I_{sat} drastically decreases while the reduction is modest after the Kr seeding.

plasmas. The ΣI_{sat} ratio also decreases in all toroidal sections in both plasmas. It should be emphasized again that the detachment in Kr+Ne seeded plasmas is sustained while the detachment in Ne seeded plasma is transient.

Plasma radiation profiles measured with the resistive bolometer arrays in Kr+Ne seeded plasma and Ne only seeded plasma are shown in FIG. 6. Here, the radiation is the power irradiated onto the bolometer arrays and $r_{eff,\ min}$ is determined as the minimum r_{eff} on the bolometer sightlines. In the Kr+Ne seeded plasma, radiation is enhanced at $|r_{eff,\ min}/a_{99}| \sim 0.8$ compared with the radiation profile in Ne only seeded plasma. It indicates that plasma radiation is enhanced at the upstream region using higher-Z impurity under the same f_{rad}. Optimal impurity seeding conditions should be investigated to obtain further radiation enhancement also at the downstream region simultaneously. It is notable that the radiation profile in the Kr+Ne seeded plasma is hollow although the path length of the sightline in the core plasma is longer than that in the edge plasma. It indicates that the accumulation of the seeded impurities toward the central plasma could be suppressed during the detachment. FIG. 7 shows the time evolution of T_e at various radial positions.
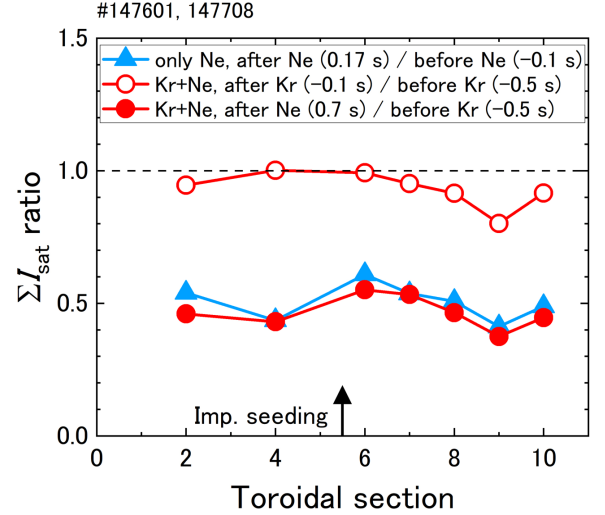
#147601, 147708

FIG. 5. toroidal profile of ΣI_{sat} ratio before impurity seeding and after impurity seeding. While toroidal asymmetry was observed after Kr seeding, ΣI_{sat} decreased in all toroidal sections after Ne seeding in both plasmas.
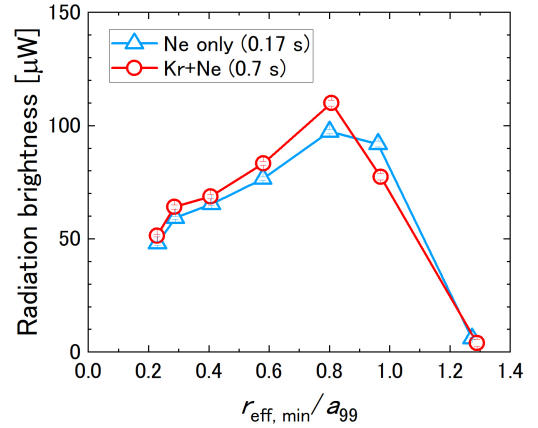

FIG. 6. Plasma radiation profiles in Kr+Ne seeded plasma and Ne only seeded plasma. Plasma radiation was enhanced at the upstream region using higher-Z impurity under the same f_{rad}.
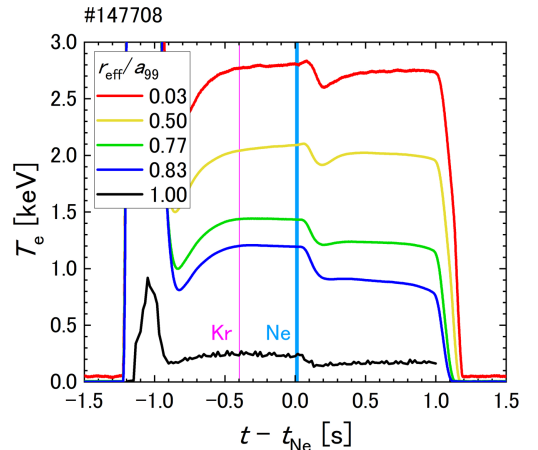
#147708

FIG. 7. time evolution of T_e profile. Reduced T_e due to Ne seeding is recovered at $|r_{eff}/a_{99}| \sim 0.8$ after $t - t_{Ne} = 0.2$ s.

While T_e decreases after the Ne seeding in all radial positions, T_e is recovered at $|r_{eff}/a_{99}| \sim 0.8$ after $t - t_{Ne} = 0.2$ s. It is consistent with the suppression of the impurity accumulation towards the central plasma.

FIG. 8. shows the radial profiles of n_e, T_e, and electron pressure, p_e, in Kr+Ne seeded plasma and in Ne only seeded plasma. Profiles are comparable at $r_{eff}/a_{99} > 0.9$ although core n_e is higher in the Kr+Ne seeded plasma. The Ne seeding amount in Ne only seeded plasma is 1.6 times that in Kr+Ne seeded plasma. Since the amount of deuterium puff is the same in both discharges, the higher core n_e in Kr+Ne seeded plasma is caused by the Kr ionization. FIG. 9 shows the relation between f_{rad} and $\tau_{E, exp}/\tau_{E, ISS04}$. f_{rad} in the Ne only seeded plasmas is plotted as the averaged value in the transient detachment and f_{rad} in the Kr+Ne seeded plasma is plotted as the averaged value in the steady state, 0.4 s $\leq t - t_{Ne} \leq 1.0$ s. In the Ne only seeded plasma, $\tau_{E, exp}/\tau_{E, ISS04}$ degrades with the increase of f_{rad}. In the Kr+Ne seeded plasma, while the detachment can be sustained, $\tau_{E, exp}/\tau_{E, ISS04}$ was 10% lower than that in the Ne only seeded plasmas under the same f_{rad}. Optimization of impurity screening may improve the confinement degradation in the Kr+Ne seeded plasma from the Ne only seeded plasmas. Moreover, n_e fluctuations can be considered as a candidate of the $\tau_{E, exp}$ degradation from $\tau_{E, ISS04}$ during the detachment phase. FIG. 10 shows the time evolutions of the n_e fluctuation profile measured with two-dimensional phase contrast imaging (PCI) [14]. Both in the Kr+Ne seeded plasma and Ne only seeded plasma, n_e fluctuation is enhanced after the Ne seeding during the detachment especially at $0.7 < |r_{eff}/a_{99}| < 0.8$. In order to improve the energy confinement during the detachment, the fluctuation should be suppressed. FIG. 11 shows the relation between the seeded impurity amount and the f_{rad}. Higher f_{rad} is obtained using Kr+Ne seeding compared with the Ne only seeded plasmas under the same seeded impurity amount. In order to sustain the detachment in Ne only seeded plasmas as long as that in Kr+Ne seeded plasma, several times Ne injection, i.e., further amount of Ne is required. It indicates that multi-species impurity seeding is competitive for steady-state operation without dilution.

3.2. Kr emission enhancement due to Ne seeding

In the Kr+Ne superimposed discharges, KrXIX emission is drastically enhanced as shown in FIG. 2 (e). On the other hand, in the Kr only seeded plasmas, radiative cooling is not effective. The reduction of edge T_e is modest and f_{rad} is up to 0.21 [5]. These results indicate that Kr ions are transported toward the upstream region in Kr+Ne superimposed discharges. FIG. 12 shows the radial profiles of seeded impurity ion emission intensity (KrXIX and NeVIII). The difference of the peak position between FIG. 6 and FIG. 12 can be considered that Kr and Ne ions with higher charge state can exist and that the spread of the bolometer sightline
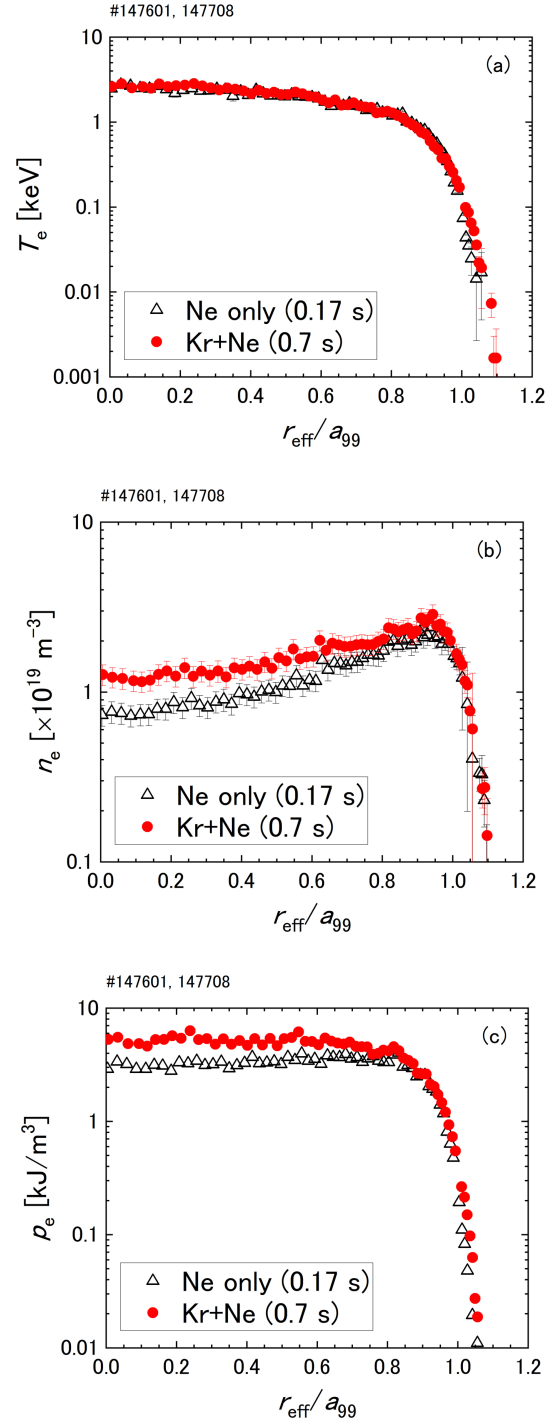

FIG. 8. Radial profiles of (a) n_e, (b) T_e, and (c) p_e in Kr+Ne seeded plasma and in Ne only seeded plasma measured with Thomson scattering. Profiles are comparable at $r_{eff}/a_{99} > 0.9$ although core n_e is higher in the Kr+Ne seeded plasma.

is larger than that of the EUV spectroscopy. While NeVIII is exhausted with the reattachment in the Ne only seeded plasma, KrXIX and NeVIII are retained at $r_{eff}/a_{99} \sim 1$ in the Kr+Ne seeded plasma. Negative radial electric field, E_r,
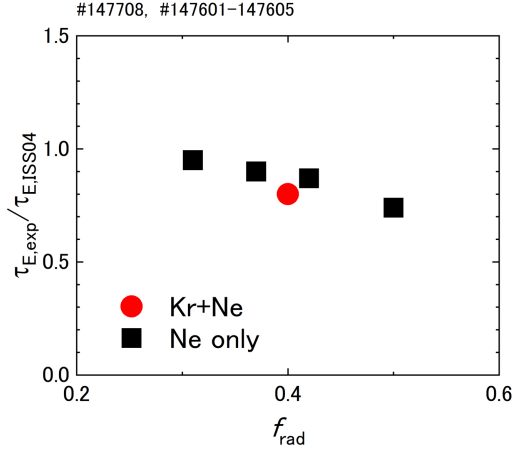
FIG. 9. Relation between f_{rad} and $\tau_{E,\,exp}/\tau_{E,\,ISS04}$. In the Kr+Ne seeded plasma, $\tau_{E,\,exp}/\tau_{E,\,ISS04}$ comparable to that in the Ne only seeded plasmas under the same f_{rad} is sustained.
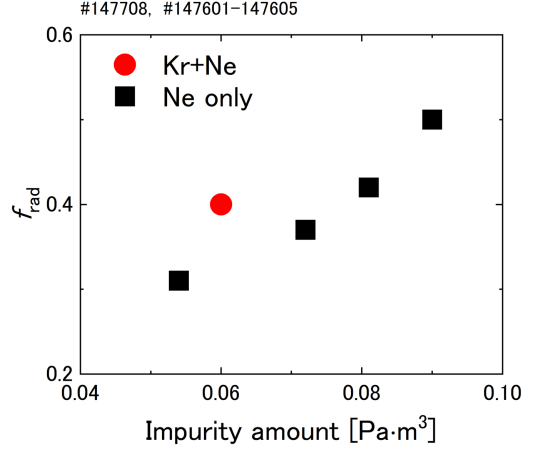

FIG. 11. Relation between the seeded impurity amount and f_{rad}. Higher f_{rad} is obtained using Kr+Ne seeding compared with the Ne only seeded plasmas.
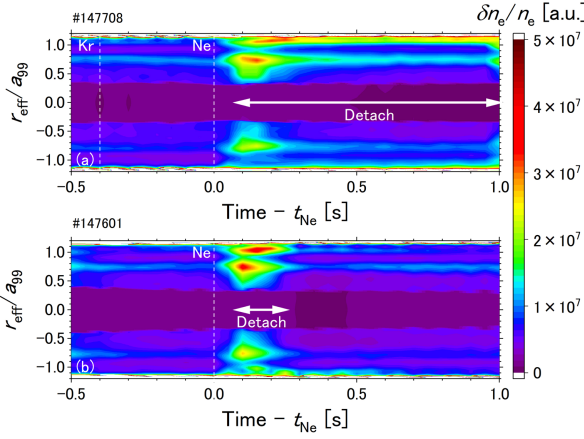

FIG. 10. Time evolutions of n_e fluctuation profile measured with two-dimensional phase contrast imaging (PCI). In the both cases, n_e fluctuation is enhanced after the Ne seeding during the detachment especially $0.7 < |r_{eff}/a_{99}| < 0.8$.

forms after $t - t_{Ne} = 0.4$ s as shown in FIG. 2 (i). It can promote the retention of the Kr ions. Although negative E_r forms also in the Ne only seeded plasma as shown in FIG. 3 (i) after $t - t_{Ne} = 0.3$ s, the plasma is almost reattached at this time.

The impurity accumulation behavior in LHD can be characterised by the relation between n_e and T_e at the LCFS ($n_{e,\,LCFS}$, $T_{e,\,LCFS}$), the so-called n-T diagram [15, 16]. In the study, the accumulation and screening of intrinsic impurities (carbon and iron) was investigated in the steady-state NBI-heated plasmas. The main gas was hydrogen while the main gas in this paper is deuterium. In the lower-$n_{e,\,LCFS}$ and higher-$T_{e,\,LCFS}$ region on the n-T diagram, impurities are screened by positive radial electric field, E_r. In the higher-$n_{e,\,LCFS}$ and lower-$T_{e,\,LCFS}$ region, impurities are also screened by friction force in the ergodic layer. In the high-power discharges, i.e., in the higher-$n_{e,\,LCFS}$ and higher-$T_{e,\,LCFS}$

region, impurities are screened by the increase of the ion temperature gradient and Mach number. Therefore, when plasmas are in a certain window on the n-T diagram, impurity accumulation occurs.

Time evolutions of $n_{e,\,LCFS}$ - $T_{e,\,LCFS}$ characteristics in the Kr+Ne superimposed discharges are shown in FIG. 13. $n_{e,\,LCFS}$, $T_{e,\,LCFS}$ are plotted every 0.1 s. The color of the symbols corresponds to the intensity of the KrXIX emission. Three cases of the discharges are plotted on FIG. 13. In the first case KrXIX emission is not enhanced after the Ne seeding (open squares). In the second case KrXIX emission is enhanced and sustained (closed circles). In the last case KrXIX is enhanced but radiatively collapsed (open triangles). Note that the amount of the seeded impurities is the same among all cases. ($n_{e,\,LCFS}$, $T_{e,\,LCFS}$) is around (0.9×10^{19} m^{-3}, 240 eV) after Kr seeding but before Ne seeding in all cases. After the Ne seeding, due to the ionization of the seeded Ne, ($n_{e,\,LCFS}$, $T_{e,\,LCFS}$) changes towards higher-$n_{e,\,LCFS}$ and lower-$T_{e,\,LCFS}$. In the stably detached discharge shown in FIG. 2, 0.2 s after the Ne seeding ($t - t_{Ne} = 0.2$ s), ($n_{e,\,LCFS}$, $T_{e,\,LCFS}$) changed to around (1.6×10^{19} m^{-3}, 150 eV). Then, the KrXIX emission is enhanced. One the other hand, in the case that KrXIX is not enhanced, $T_{e,\,LCFS}$ reduction is smaller than that in the other two cases. In the radiatively collapsed case, the $n_{e,\,LCFS}$ increase is higher than that in the other two cases. These results lead to two conditions; (i) when $T_{e,\,LCFS}$ is reduced below $\sim$ 150 eV by the Ne seeding, KrXIX is enhanced and (ii) when the $n_{e,\,LCFS}$ increases above 2×10^{19} m^{-3} after the Ne seeding, the plasma radiatively collapses.

The behavior of KrXIX emission enhancement is various although the amount of the seeded Kr and Ne are the same among the discharges. It indicates that impurity transport is different among the three cases. $n_{e,\,LCFS}$ and $T_{e,\,LCFS}$ after Kr seeding but before Ne seeding in all cases are similar. However, the $n_{e,\,LCFS}$ and $T_{e,\,LCFS}$ are near the border between
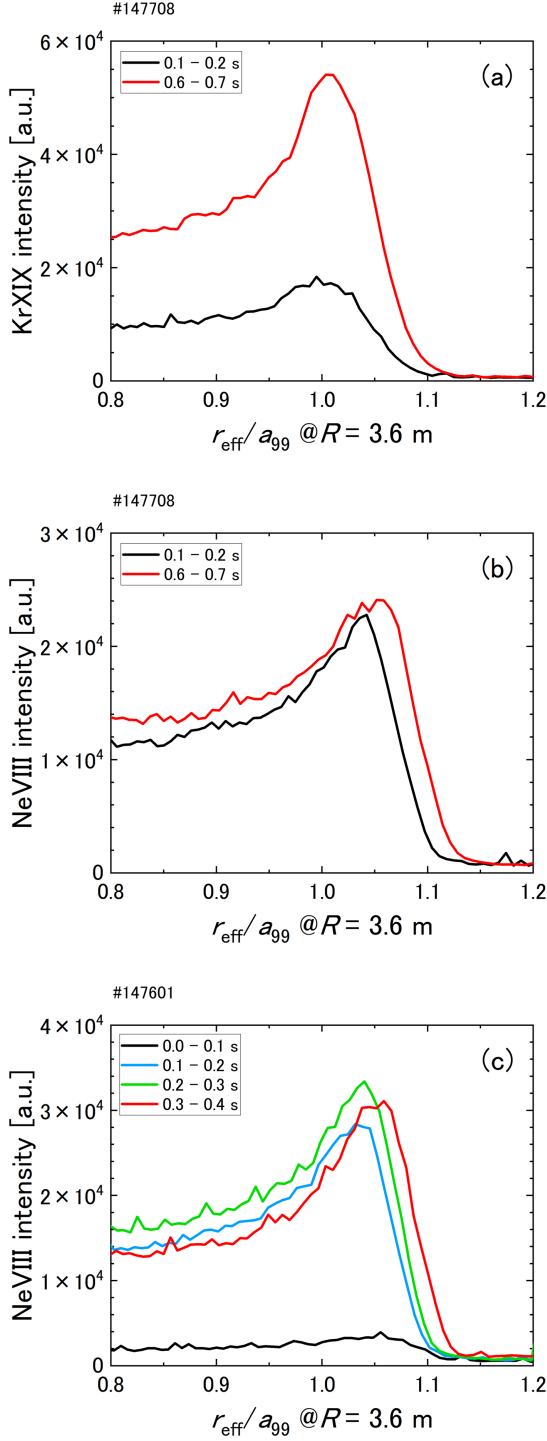
#147708 (a)

#147708 (b)

#147601 (c)

FIG. 12. Radial profiles of seeded impurity ion emission (KrXIX, NeVIII) intensity in Kr+Ne seeded plasma (a, b) and in Ne only seeded plasma (c). While NeVIII is exhausted with the reattachment in the Ne only seeded plasma, KrXIX and NeVIII are retained at $r_{eff}/a_{99} \sim 1$ in the Kr+Ne seeded plasma.

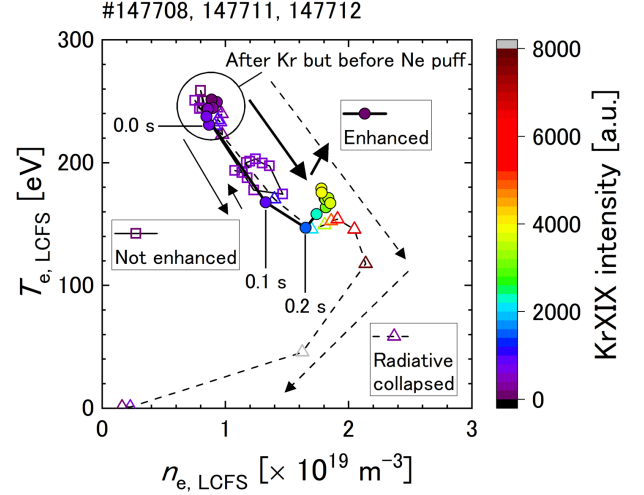*FIG. 13. Relation between $n_{e, LCFS}$, $T_{e, LCFS}$, and KrXIX emission in Kr+Ne superimposed seeded discharges. Although the amount of the seeded impurities is the same, plasma response is different depending on the $n_{e, LCFS}$ and $T_{e, LCFS}$ of the background plasmas.*

evaluated for carbon and iron. These results imply that a small difference in the $n_{e, LCFS}$ - $T_{e, LCFS}$ characteristics before the Ne seeding strongly affects the response of the Kr enhancement. The relation between $n_{e, LCFS}$ 0.1 s before the Ne seeding, $n_{e, LCFS}$ (t - t_{Ne} = -0.1 s), and $\Delta n_{e, LCFS}$, $\Delta T_{e, LCFS}$, ΔKrXIX, and ΔNeVIII are shown in FIG. 14. Smaller $n_{e, LCFS}$ makes the larger impurity screening and larger $n_{e, LCFS}$ makes the larger impurity penetration. The differences are determined by the subtraction of those 0.1 s before Ne seeding from those 0.2 s after Ne seeding. $\Delta n_{e, LCFS}$ increases with the increase of $n_{e, LCFS}$ (t - t_{Ne} = -0.1 s). Since the amounts of the seeded Kr and Ne are the same, enhancement of Ne ionization due to an increase of Ne penetration at the ergodic layer can be considered as one of the candidates for the increase of $\Delta n_{e, LCFS}$. When $n_{e, LCFS}$ (t - t_{Ne} = -0.1 s) is below 0.8×10^{19} m^{-3}, KrXIX emission is not enhanced while the NeVIII emission intensity increases. When $n_{e, LCFS}$ (t - t_{Ne} = -0.1 s) is above 0.8×10^{19} m^{-3}, further $\Delta T_{e, LCFS}$ decrease is observed and KrXIX emission intensity is enhanced while the NeVIII emission intensity saturates. It indicates that ionization of Kr atoms and transport of Kr ions changes at $n_{e, LCFS}$ (t - t_{Ne} = -0.1 s) $\sim 0.8 \times 10^{19}$ m^{-3}.

In order to investigate the momentum balance, e.g. friction force and thermal force, in the ergodic layer, data of ion temperature and effective ion charge is required. E_r measurement in core plasma is also required to investigate the mechanism to suppress the impurity accumulation toward the central plasma. Simulation study is also needed for the discussion. Control of the edge profile using divertor pumping and feedback control using fast Thomson scattering and/or ECH in the edge plasma are required to obtain further
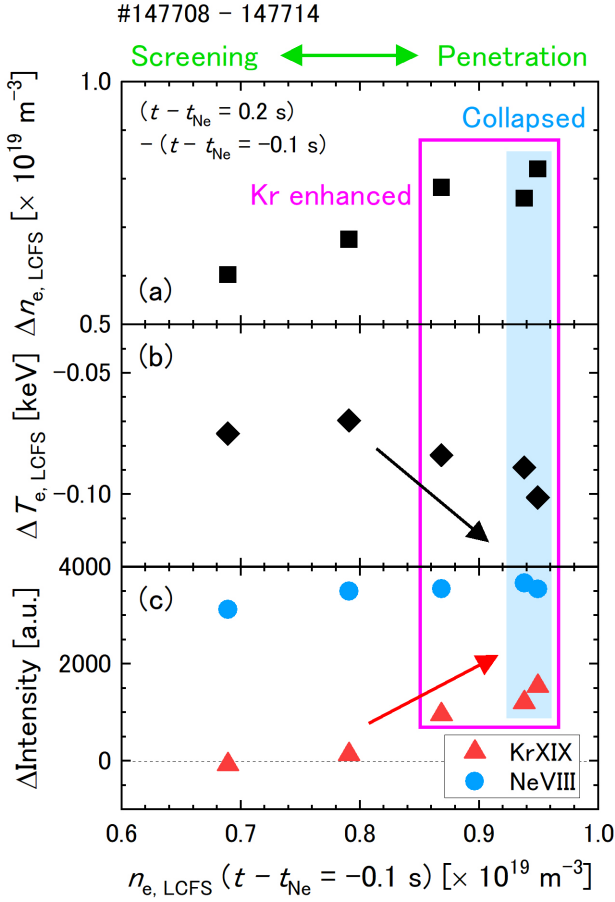
screening and accumulation areas in the lower-$n_{e, LCFS}$ and higher-$T_{e, LCFS}$ region [15, 16] although these areas are

#147708 − 147714

FIG. 14. Background $n_{e, LCFS}$ dependence of (a) $\Delta n_{e, LCFS}$, (b) $\Delta T_{e, LCFS}$, (c) $\Delta KrXIX$, and $\Delta NeVIII$. When the background $n_{e, LCFS}$ is above 0.8×10^{19} m^{-3}, further $T_{e, LCFS}$ reduction and KrXIX enhancement occurres.

radiation enhancement and further sustainment of the detachment.

4. Summary

Multi-species impurity seeding is an advanced operation scenario to mitigate the divertor heat load for the realization of future fusion reactors. In the Large Helical Device (LHD), divertor detachment is successfully sustained using higher-Z (Kr) and lower-Z (Ne) superimposed seeding. Emission from Kr impurities is drastically enhanced if it is followed by Ne seeding. Plasma radiation can be enhanced even at the upstream region in the edge plasma compared with Ne only seeded plasmas with suppression of impurity accumulation toward the central plasma. The characteristics of divertor heat load reduction and energy confinement are comparable between the Kr+Ne seeding and Ne only seeding under the same f_{rad}. However, while the detachment in Ne only seeding is transient, the detachment in Kr+Ne seeding is stable. It indicates that multi-species impurity seeding can be competitive for steady-state operation although further investigation is desired about the balance between divertor

heat load reduction, impurity screening, and confinement degradation. The Kr emission enhancement is strongly affected by $n_{e, LCFS}$ and $T_{e, LCFS}$ resulting in impurity penetration. Feedback control of these parameters using fast Thomson scattering and/or ECH in the edge plasma may be helpful to obtain further radiation enhancement and further sustainment of the detachment.

References

[1] GAŁĄZKA, K. *et al.* 2018 *Contrib. Plasma Phys.* **58** 751-757
[2] KALLENBACH, A. *et al*, 2012 *Nucl. Fusion* **52** 112003
[3] EFFENBERG, F *et al*, 2019 *Nucl. Fusion* **59** 106020
[4] MASUZAKI, S. *et al.* 2013 *J. Nucl. Mater.* **438** S133
[5] MUKAI, K. *et al.* 2015 *Nucl. Fusion* **55** 083016
[6] TANAKA, H. *et al.* 2017 *Nucl. Mater. Energy* **12** 241-246
[7] MUKAI, K. *et al.* 2020 *Plasma Fusion Res.* **15** 1402051
[8] ZHANG, H. *et al.* 2015 *Jpn. J. Appl. Phys.* **54** 086101
[9] SCHWOB, J. L. *et al.*1987 *Rev. Sci. Instrum.* **58** 1601
[10]   SUZUKI, C. *et al.* 2015 *J. Nucl. Mater.* **463** 561-564
[11]   SUZUKI, C. *et al.* 2019 *Nucl. Mater. Energy* **19** 195-199
[12]   YAMADA, H. *et al.* 2005 *Nucl. Fusion* **45** 1684
[13]   TANAKA, H. *et al.* 2018 *Plasma Phys. Control. Fusion* **60** 125001
[14]   TANAKA, K. *et al.* 2008 Rev. Sci. Instrum. 79 10E7021
[15]   NAKAMURA, Y. *et al.* 2014 *Plasma Phys. Control. Fusion* **56** 075014
[16]   NAKAMURA, Y. *et al.* 2017 *Nucl. Fusion* **57** 056003